Blob-hole correlation model for edge turbulence and comparisons with NSTX GPI data

J R Myra,[1] S J Zweben[2] and D A Russell[1]

[1] *Lodestar Research Corporation, Boulder, CO, USA*
[2] *Princeton Plasma Physics Laboratory, Princeton, NJ*

February 2018

submitted to Plasma Phys. Control. Fusion

Blob-hole correlation model for edge turbulence and comparisons with NSTX GPI data

J R Myra,[1] S J Zweben[2] and D A Russell[1]

[1] *Lodestar Research Corporation, Boulder, CO 80301, USA*
[2] *Princeton Plasma Physics Laboratory, Princeton, NJ 08540, USA*

Abstract

Gas puff imaging (GPI) observations made in NSTX [Zweben S J, *et al.*, 2017 Phys. Plasmas **24** 102509] have revealed two-point spatial correlations of edge and scrape-off layer turbulence in the plane perpendicular to the magnetic field. A common feature is the occurrence of dipole-like patterns with significant regions of negative correlation. In this paper, we explore the possibility that these dipole patterns may be due to blob-hole pairs. Statistical methods are applied to determine the two-point spatial correlation that results from a model of blob-hole pair formation. It is shown that the model produces dipole correlation patterns that are qualitatively similar to the GPI data in several respects. Effects of the reference location (confined surfaces or scrape-off layer), a superimposed random background, hole velocity and lifetime, and background sheared flows are explored and discussed with respect to experimental observations. Additional analysis of the experimental GPI dataset is performed to further test this blob-hole correlation model. A time delay two-point spatial correlation study did not reveal inward propagation of the negative correlation structures that were postulated to correspond to holes in the data nor did it suggest that the negative correlation structures are due to neutral shadowing. However, tracking of the highest and lowest values (extrema) of the normalized GPI fluctuations shows strong evidence for mean inward propagation of minima and outward propagation of maxima, in qualitative agreement with theoretical expectations. Other properties of the experimentally observed extrema are discussed.

1. Introduction

Understanding edge and scrape-off layer (SOL) physics in magnetically confined plasmas is an important scientific challenge and one that is of great practical interest for the development of fusion power [1]. The edge or closed flux surface region near the separatrix of a tokamak provides the final layer of confinement for the contained plasma within. Turbulent transport in this region may thus be expected to have an important influence on the overall confinement properties of the device. In the SOL, or open flux surface region outside the separatrix, particles and heat are transported by turbulence across magnetic field lines as the plasma flows along field lines to the divertor target or to intercepting limiters. In this region plasma turbulence may contribute to the physics that sets the width of the heat flux channel [2-5] and hence to the power flux impinging on material surfaces. Rapidly convecting turbulent structures in the form of blob-filaments [6-9] may travel long distances across the SOL [10-13] and eventually strike the main chamber walls or other hardware causing plasma material interactions. At both the main chamber walls and the divertor target plates, interactions such as impurity sputtering, erosion, and recycling, can impact device performance and component longevity [1].

Coherent structures in edge turbulence were first observed many years ago using probes [14], a diagnostic that continues to provide valuable single point (per probe) measurements from which density, temperature and potential fluctuations can be inferred [15, 16]. For obtaining a two-dimensional (2D) dynamic view of plasma fluctuations, the technique of gas puff imaging (GPI) has been developed and employed on many plasma devices. A review of the technique and additional references on fast imaging in magnetic fusion devices may be found in Ref. [17]. On the NSTX spherical torus, GPI was used routinely to characterize edge and SOL turbulence [18]. Much work in the area of modeling and computer simulation remains in order to achieve a satisfactory understanding of this data.

One analysis technique that provides important clues about the structure of boundary plasma turbulence is that of 2D spatial cross-correlation. The 2D radial vs. poloidal cross-correlation functions of edge plasma turbulence were recently measured near the outer midplane with the GPI diagnostic on NSTX [19]. A common feature that was observed is the occurrence of dipole-like patterns in the cross-correlation function with significant regions of negative correlation. Possible explanations that were discussed include the formation and propagation of blob-hole pairs [19] and the neutral density 'shadowing' effect in GPI [17,20,21]. In this paper, we present a more detailed

examination of the possibility that the observed negative correlations could be due to blob-hole pairs arising from plasma turbulence. Our approach is two-fold, consisting of both modeling of blob-hole dynamics and additional examinations of the experimental data in a search for holes and their properties.

The modeling approach taken in the present work is designed to gain insight into the qualitative connection of physical processes to the experimental data using rather simple conceptual semi-analytic methods. In particular, here we proposed a specific plausible model for the creation and propagation of blob-hole pairs and investigate the degree to which such a model can qualitatively describe the experimentally observed correlation patterns. Our model consists of both a deterministic function for the evolution of an individual blob-hole pair, and a statistical component for construction of the correlation functions. The main statistical assumptions are that the amplitude of the blob-hole pair is random, their creation time is Poisson distributed [22] and they sit on top of a temporal background of Gaussian white noise which is spatially correlated. The white noise is meant to simulate the usual background component of edge turbulence which does not consist of blob/hole pairs.

The propagation dynamics of isolated blobs under controlled conditions has been described by basic theory and modeling with some validation from fundamental physics experiments, especially in linear devices [7, 8]. In simple terms, a blob or blob-filament is defined as flux tube containing higher density and pressure than the surrounding plasma. Blobs preferentially propagate outward in major radius, i.e. to lower magnetic field B. The reason is attributed to binormal (approximately poloidal) charge polarization of the blob resulting from grad-B and curvature drift currents which lead to an internal blob poloidal electric field E_y and a subsequent radial $E_y \times B$ drift. Holes, on the other hand, are filamentary structures which contain less pressure than the surrounding plasma. As a blob propagates away from the place where it was formed, it leaves behind a void or hole. The same mechanism that leads to outward blob propagation causes holes to move inward in major radius: the grad-B and curvature drift currents external to the hole charge polarize it in the opposite sense to that of a blob. The reversal of the internal electric field in a hole or void was demonstrated by probe measurements on NSTX [16].

Refinements to the theory of blob motion have included, for example, such effects as parallel electron dynamics and other 3D effects [23-25], magnetic shear [26], ion temperature [27-29], ion kinetic effects [30-32] and density gradients [33,34]. The dynamics of seeded blobs observed in some of the computational models have recently been compared with basic plasma physics experiments [35]. These additional

3

refinements are important for quantitative work, but they leave intact the basic qualitative feature of radial propagation central to the simple modeling of spatial correlations considered here.

While there has been some analytical progress in understanding the nonlinear generation of blobs from drift wave theory [36] a general description of the generation of coherent structures from underlying turbulence at present requires either numerical turbulence simulations or statistical models. On the simulation side, a number of models describing SOL turbulence with varying degrees of sophistication and generality have been developed and in many cases compared with experiments [37-44]; significant progress is underway in this modeling effort. Statistical models have also been developed and shown to provide descriptions of many features of the experimental data including a skewness-kurtosis relationship, waiting time, amplitude, and spectral distributions [22, 45, 46]. These models are also being extended in order to describe turbulence-sustained SOL profiles [47, 48]. In this paper we employ some basic statistical properties and techniques applicable to edge turbulence [49] in conjunction with our proposed blob-hole model to evaluate the resulting cross-correlation function. We are interested in knowing whether the theoretical blob-hole model can yield correlations that are similar to the NSTX GPI data, in particular with respect to the observed negative correlations and dipole patterns.

Previous measurements of correlation functions in edge turbulence were reviewed in Ref. [19]. Holes in edge plasma turbulence were first identified in the DIII-D tokamak as unusually large negative-going fluctuations in Langmuir probe ion saturation current measurements [10]. The probability distribution function (PDF) of these signals showed a negative skewness just inside the separatrix, whereas the skewness became increasingly positive farther out into the SOL due to blobs. Holes have also been seen as negative skewness in edge probe measurements of many other tokamaks, for example in JET [50], HL-2A [51], ASDEX-Upgrade [52], EAST [53], NSTX [16], and in a large database of stellarator and tokamak edge turbulence [54]. The hole radial velocity was measured to be inward using conditional sampling of probe signals from the tokamaks DIII-D [10], JET [50], HL-2A [51], NSTX [16], and in 6 out of 9 cases examined in [54], whereas the blob velocity is almost always radially outward [8]. Negative-going structures are clearly seen in GPI images, but the negative skewness associated with holes is almost never seen in GPI data [55], although the statistics for blobs is similar among various devices. The 2D structure of blobs and holes was measured using conditional averaging of probes on the linear device LAPD [56], where the hole structure appeared to be more extended in

the poloidal direction than the blob structure. Imaging measurements of negative-going density structures have also been made on LAPD [57] and in the TORPEX toroidal device [58]. In this paper we supplement previous measurements of hole structures by examining, in a GPI dataset on NSTX, the properties of negative correlation regions inside the separatrix, and the statistics, velocity and locations of minima in the GPI fluctuations using a tracking technique.

The plan of our paper is as follows. Basic theoretical background on the statistical assumptions and methods is given in Sec. 2. A model for the creation and propagation of blob-hole pairs is presented in Sec. 3. In Secs. 4 and 5 the results of the proposed model for spatial correlations in one and two dimensions are given. In Sec. 6 an experimental inquiry into the propagation of holes and fluctuation minima in the GPI data is presented. Finally Sec.7 provides a discussion and conclusions.

2. Statistical assumptions and methods

Let $S(\mathbf{x},t)$ represent an experimental measurement of the space and time dependence of some signal such as the GPI light intensity fluctuations, which are taken as a proxy for the plasma density fluctuations. The spatial two-point correlation function measured in Ref. [19] and considered in the present modeling work is defined as

$$C_{12} = \frac{\left\langle\!\left\langle \tilde{S}_1 \tilde{S}_2 \right\rangle\!\right\rangle}{S_{1,rms}S_{2,rms}} \tag{1}$$

where for j = 1 or 2

$$\tilde{S}_j = S(\mathbf{x}_j,t) - \left\langle\!\left\langle S(\mathbf{x}_j,t) \right\rangle\!\right\rangle, \tag{2}$$

$$S_{j,rms} = \left\langle\!\left\langle \tilde{S}_j^2 \right\rangle\!\right\rangle^{1/2}, \tag{3}$$

and $\mathbf{x}_1$ and $\mathbf{x}_2$ are the spatial points in question, also referred to as the reference and observation points. Here, the double angular bracket <<…>> implies a long-time average (data) or a statistical ensemble average (theoretical model).

The correlation C_{12} defined by Eq. (1) ranges from $C_{12} = 1$ (e.g. for $x_1 = x_2$) meaning perfectly correlated signals to $C_{12} = -1$ meaning perfectly anti-correlated signals, $S_2 = -S_1$, while $C_{12} = 0$ implies no correlation.

In the theoretical model, the statistical ensemble average is an average over individual "events" that correspond to the passing of a single blob or hole perturbation

past the observation point. The distribution of events in time is assumed to be governed by a Poisson process, an assumption which is justified by experimental data [22]. For a Poisson process with rate μ events/time, the statistical averages may be calculated following Ref. [49]. In particular they are related to the time integrals over individual events as follows

$$\left\langle\left\langle S_j \right\rangle\right\rangle \equiv \mu \int dt\, f_j(t) = \left\langle f_j \right\rangle \tag{4}$$

$$\left\langle\left\langle S_1 S_2 \right\rangle\right\rangle = \left\langle f_1 f_2 \right\rangle + \left\langle f_1 \right\rangle\left\langle f_2 \right\rangle \tag{5}$$

$$\left\langle\left\langle \tilde{S}_1 \tilde{S}_2 \right\rangle\right\rangle = \left\langle f_1 f_2 \right\rangle \tag{6}$$

$$S_{j,rms} = \left\langle f_j^2 \right\rangle^{1/2} \tag{7}$$

Thus S is a statistical superposition of individual events, f is the time history of one event where f(t) vanishes outside a finite localized time interval, and <…> is a time average over a single event weighted by μ, i.e. a short-hand notation for $\mu \int dt$. As will become explicit in the next section, the time of occurrence of the blob-hole event is a random Poisson variable. Under these assumptions and definitions, theoretical correlation functions may be calculated by evaluating deterministic integrals over time once the time profile of an individual event is specified. This will be done in Sec. 3.

Inserting the preceding definitions into Eq. (1) results in

$$C_{12} = \frac{\left\langle f_1 f_2 \right\rangle + r_{rms}^2\, \eta_{12}}{\left(\left\langle f_1^2 \right\rangle + r_{rms}^2\right)^{1/2}\left(\left\langle f_2^2 \right\rangle + r_{rms}^2\right)^{1/2}} \tag{8}$$

where we have added to S($\mathbf{x}$,t) a Gaussian distributed white noise function $\tilde{\eta}(\mathbf{x},t)$, assumed to have zero mean, a spatially constant rms amplitude, a spatial correlation length σ_n and a two-point spatial correlation function given by

$$\eta_{12} = e^{-\left|\mathbf{x}_1 - \mathbf{x}_2\right|^2 / 2\sigma_n^2} . \tag{9}$$

The noise level $<<\tilde{\eta}^2>>$ is prescribed by the value of

$$r_{rms}^2 = \frac{\left\langle\left\langle \tilde{\eta}^2 \right\rangle\right\rangle}{\left\langle\left\langle A^2 \right\rangle\right\rangle} \tag{10}$$

where A is the amplitude of a blob-hole event, subsequently to be taken as exponentially distributed.

We will employ this noise parameter to quantify decorrelations which are present in the experimental data. Here "noise" could represent a variety of processes other than the blob-hole pair dynamics that is explicitly modeled, e.g. turbulent structures that happen to pass through the observation point, but originate from a wide variety of locations, due to random variations in their trajectories.

3. Blob-hole model

The birth and propagation of a single blob-hole pair will be considered as an individual event. To derive the function f($\mathbf{x}$,t) required in Eq. (8) we begin with the continuity equation for the plasma density

$$\frac{\partial n}{\partial t} + \frac{n}{\tau} + \mathbf{v} \cdot \nabla n = 0 \tag{11}$$

Here τ is the lifetime of a structure (blob or hole) and $\mathbf{v}$ is the total velocity of that structure in the lab frame,

$$\mathbf{v} = \mathbf{v}_j - \alpha x \mathbf{e}_y \tag{12}$$

where $\mathbf{v}_j$ is the velocity of the structure relative to the background and $\alpha x \mathbf{e}_y$ is the background sheared flow. The sheared flow is in the y (approximately poloidal) direction and x is a radial coordinate. For convenience, it is assumed that we work in the frame of the background flow at x = 0, since an overall frame change will have no effect on the correlations.

The method of characteristics applied to Eq. (11) gives the solution

$$n(x,y,t) = e^{-t/\tau_j} n_0[x - v_{jx}t, y - (v_{jy} - \alpha x)t - \alpha v_{jx}t^2/2)] \tag{13}$$

where $n_0(x, y, t)$ is the initial condition. For this, we take a blob/hole pair, i.e. the superposition of

$$n_{0j}(x,y) = s_j \exp\left(-\frac{(x-x_0)^2}{2\delta_x^2} - \frac{(y-y_0)^2}{2\delta_y^2}\right) \tag{14}$$

where $s_j = +1$ for a blob and -1 for a hole. The total blob/hole event (assumed to exist on top of a constant background density which does not enter the correlation function) is then

$$\begin{aligned} f(x,y,t) = A\, n_0(x - v_{bx}\Delta t, y - (v_{by} - \alpha x)\Delta t - \alpha v_{bx}\Delta t^2/2)\exp(-\Delta t/\tau_b) \\ - A\, n_0(x - v_{hx}\Delta t, y - (v_{hy} - \alpha x)\Delta t - \alpha v_{hx}\Delta t^2/2)\exp(-\Delta t/\tau_h) \end{aligned} \tag{15}$$

where $\Delta t = t - t_0 > 0$, t_0 is a random (Poisson distributed) blob-hole birth time. The amplitude A is taken to be a random variable with an exponential distribution, consistent with experimental results [45,46]. Since the correlation function is independent of the overall normalization of amplitudes, we may take $<<A>> = 1$. Then, for an exponential distribution $<<A^2>> = 2$.

Thus the random variables of the model are t_0, A and the Gaussian noise $\tilde{\eta}$. Other model parameters including $\mathbf{v_b}$, α, τ_b, τ_h, x_0, y_0, δ_x, δ_y and σ_n, together with the statistical parameters μ and r_{rms} are inputs.

The model given by Eqs. (14) and (15) describes the birth, growth and propagation of a blob-hole pair created continuously from zero at $\Delta t = 0$. Note that Eq. (13) only applies for $\Delta t \geq 0$; for $\Delta t < 0$ we take $f = 0$. Figure 1 illustrates the formation of this pair at successive times using the 1D base case parameters given in Sec. 4, Table I. As time progresses the blob propagates to the right (outward) while the hole propagates to the left (inward) and decays.

The propagation of a blob-hole pair on a background sheared flow using Eq. (15) is illustrated in Fig. 2 using the 2D base case parameters given in Sec. 5. except that for the figure we take $\alpha = 0.3$.
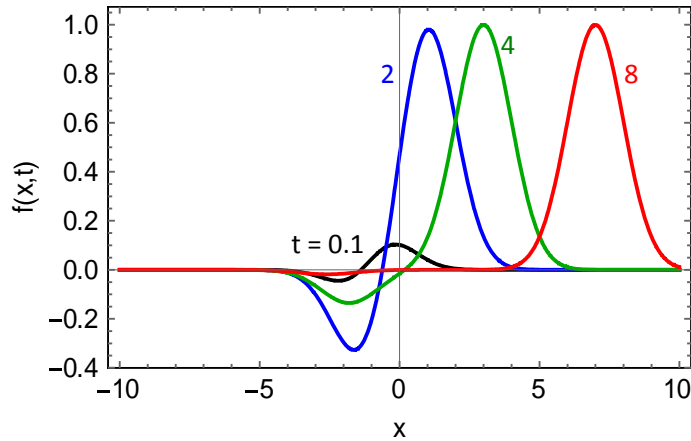

Fig. 1 Formation of a blob-hole pair. The function f(x,t) given by Eq. (15) is illustrated at various normalized times. The pair grows continuously from zero at t = 0. 1D base case parameters are employed for this example. See Sec. 4 for space and time normalizations.
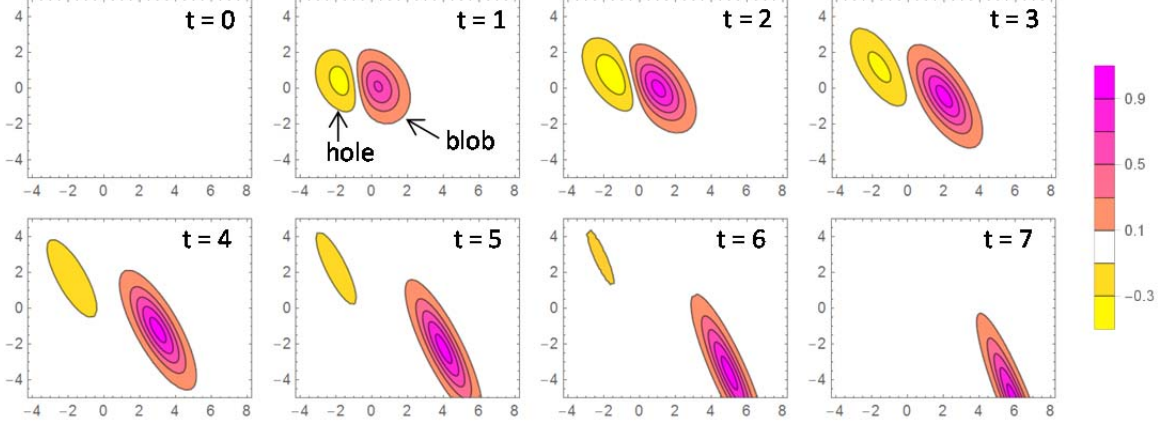
Fig. 2 Snapshots of propagation of a blob-hole pair on a background sheared flow at various normalized times. Base case parameters are employed except for $\alpha = 0.3$. See Sec. 4 for space and time normalizations. The horizontal coordinate (x) is radial, and the vertical coordinate (y) is binormal (approximately poloidal). The blob peak amplitude is A = 1 and regions with |f(x,t)| < 0.09 are rendered as white.

4. Spatial correlations in 1D

To generate spatial correlation functions in 1D, we use the function $f(x,0,t)$ defined by Eq. (15) in Eq. (8) with $f_1 = f(x_1,0,t)$ and $f_2 = f(x_2,0,t)$ where $x_1 = x_{ref}$ is held fixed and the observation point x_2 is varied. Here in Sec. 4, and also in Sec. 5, the correlation functions are computed semi-analytically by performing the required time integrations over $f(x,y,t)$ (i.e. the evaluations in these sections were not performed from random statistical samples requiring a specific number of blobs). The result is shown in Fig. 3 for the set of 1D base case parameters given in Table 1. For these 1D studies, there is no sheared flow, i.e. $\alpha = 0$. The parameters are given in dimensionless units which normalize spatial scales to the blob size parameter δ_x and velocities to the blob radial velocity v_{bx}, therefore time is normalized to the transit time of a blob moving past a fixed reference point. The choice of Poisson parameter $\mu = 0.1$ corresponds to intermittency, i.e. the average waiting time between blobs is 10 times the transit time of an individual blob. The hole is assumed to move inward at a slower speed than the blob moves

outward, motivated by the fact that the hole is moving into a higher pressure background plasma and background plasma slows the propagation of coherent structures [8]. The hole lifetime is assumed to be short because parallel flow on closed flux surfaces from the background high pressure plasma should fill in the void rather quickly.

Table 1. Dimensionless base case parameters for 1D studies

Symbol	Default	Comment
x_0	−1.	creation location
δ_x	1.	blob-hole spatial size
v_{bx}	1.	blob velocity
τ_b	∞	blob lifetime
v_{hx}	−0.2	hole velocity
τ_h	2.	hole lifetime
r_{rms}	0.2	relative noise amplitude
σ_n	1.	noise spatial correlation
μ	0.1	Poisson blob-hole creation rate

In Fig. 3 the arbitrary zero of x is meant to correspond heuristically to the separatrix and the blob-hole creation location at x = −1 is chosen to be just inside the separatrix. It can be seen that when x_{ref} is located inside the separatrix, the hole appears as a positively correlated region and the blob is a negatively correlated region. When x_{ref} is located outside the separatrix, the blob appears as a positively correlated region and the hole is a negatively correlated region. Thus the correlation pattern flips as the reference point moves across the separatrix. This feature is also characteristic of the NSTX data [19].
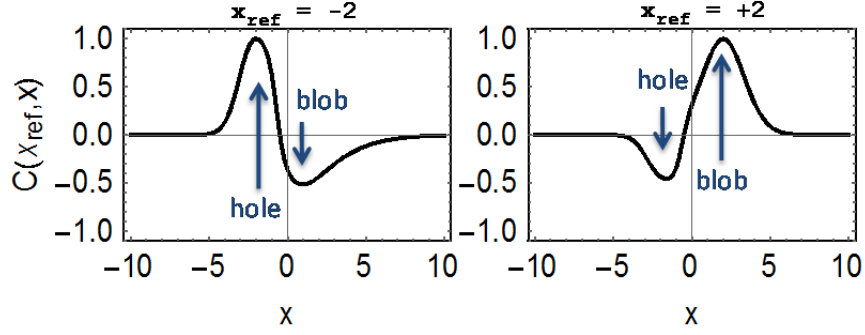
Fig. 3 Correlations in 1D for the base case parameters

Variations of the 1D correlations with some of the model parameters are shown in Fig. 4. The main conclusions from this figure are as follows: (a) noise decreases the magnitude of negative correlations; (b) a larger noise spatial correlation length broadens the response, especially for $x < -4$ where the hole signal is weak and the correlation mainly reflects that of the noise with itself; (c) increasing the reference location reduces the minimum negative correlation because the hole has decayed away when the blob reaches the far SOL; (d) increasing the magnitude of the hole velocity shifts the negative correlation as expected (right panel); (e) increasing the hole lifetime broadens and deepens the negative correlation. The right panel of Fig. 4(c) is especially interesting as it qualitatively reflects NSTX data: for reference locations deep in the SOL, negative correlations are less evident.

The competition between the background noise level and the blob-hole pair creation rate μ is illustrated in Fig. 5. Base case parameters are used except for μ. Also for this illustration $x_{ref} = 2$; therefore, we are considering the negative correlation caused by the hole. The results are given at the minimum of $C_{12} \equiv C_{min}$ which occurs near $x = -1$. In general, noise suppresses the negative correlations, reducing $|C_{min}|$. Larger μ implies more coherent blob-hole pairs per unit time, and somewhat mitigates the effect of noise. Also shown is the effect of the blob lifetime, changed from the base-case value of ∞ to 2 for the dashed curve. Thus $|C_{min}|$ decreases with background noise, with reduced blob lifetime and with a reduced blob-hole production rate.

The reduction of $|C_{min}|$ with increased noise level may correspond to one of the experimental observations. In Fig. 18(b) of Ref. [19] it is shown that when more blobs are detected per unit time, i.e. when the turbulence is stronger, $|C_{min}|$ is reduced, eventually approaching zero. In the model, stronger turbulence corresponds to (i) a larger μ (more blob-hole pairs per unit time with signals at both the reference and observations points); and (ii) a larger background noise level r_{rms} (more uncorrelated signals at the reference

and observations points). If blobs are created at random locations and emitted over a large range of velocity vector angles, we might expect (ii) to eventually dominate which would explain the experimentally observed trend.
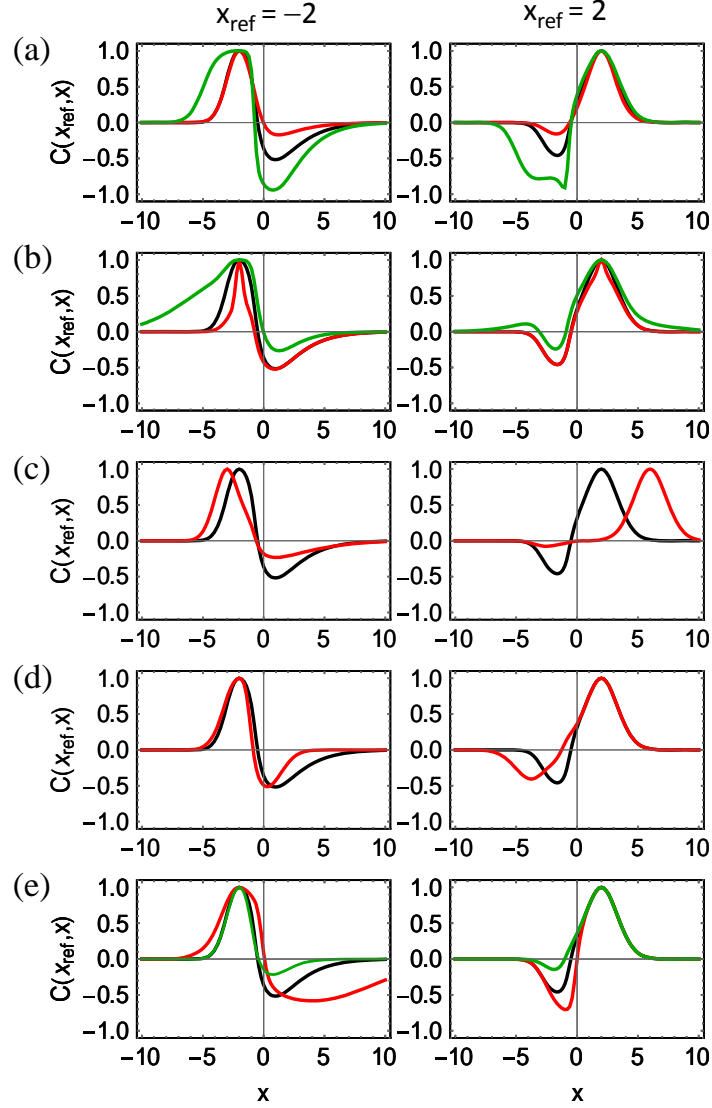

Fig. 4 Variations of the 1D correlations with some of the model parameters for reference points inside (left panels) and outside (right panels) the separatrix. Parameters are as follows: (a) r_{rms} = 0.5 (red), 0.2 (black), 0 (green); (b) σ_n = 0.25 (red), 1.0 (black), 4 (green); (c) left: x_{ref} = −3 (red), −2 (black) and right: +2 (black) +6 (red); (d) v_{hx} = −1 (red) and −0.2 (black); and (e) τ_h = ∞ (red), 2 (black), 1 (green). Black curves correspond to the base case parameters.
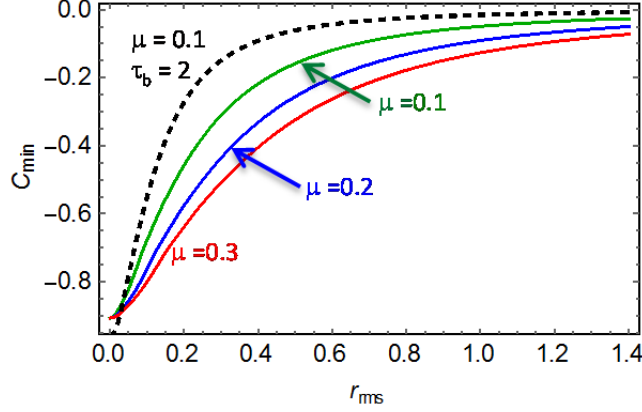
Fig. 5 Competition between background noise level r_{rms} and blob-hole creation rate μ on the magnitude of the minimum correlation C_{min}. Also shown in the dashed line is the effect of the blob lifetime.

5. Spatial correlations in 2D

Although the 1D correlation studies capture much of the content of the model, the correlation patterns in 2D are better suited to visual comparisons with the published experimental data, and also exhibit the effect of a background sheared flow. The base case parameters for the 2D studies are the same as listed in Table 1 together with the additional parameters listed in Table 2. In the 2D work, y is the poloidal coordinate.

5.1 Effect of velocity shear

The effect of velocity shear on the 2D correlation functions is illustrated in Fig. 6. In these plots the red/green region is the positive self-correlation of the blob or hole and the blue/cyan region is the negative cross-correlation of the blob with the hole (or vice versa). The upper panels, without a background sheared flow, exhibit characteristic dipole patterns, similar to the NSTX observations but with positive (red) and negative (blue) correlation regions that are more circular than the experimental data. The lower panels, for the sheared flow case with $\alpha = 0.3$, show how the shear affects the correlation pattern. This effect is stronger when the reference location is in the SOL, sensing the blob. This is because the hole has a relatively short lifetime, and during this time not much shearing can occur. Note that the shearing rate in the model is constant spatially, a feature which is unlikely to apply very well to the experiment.

13

Table 2. Additional base case parameters for 2D studies

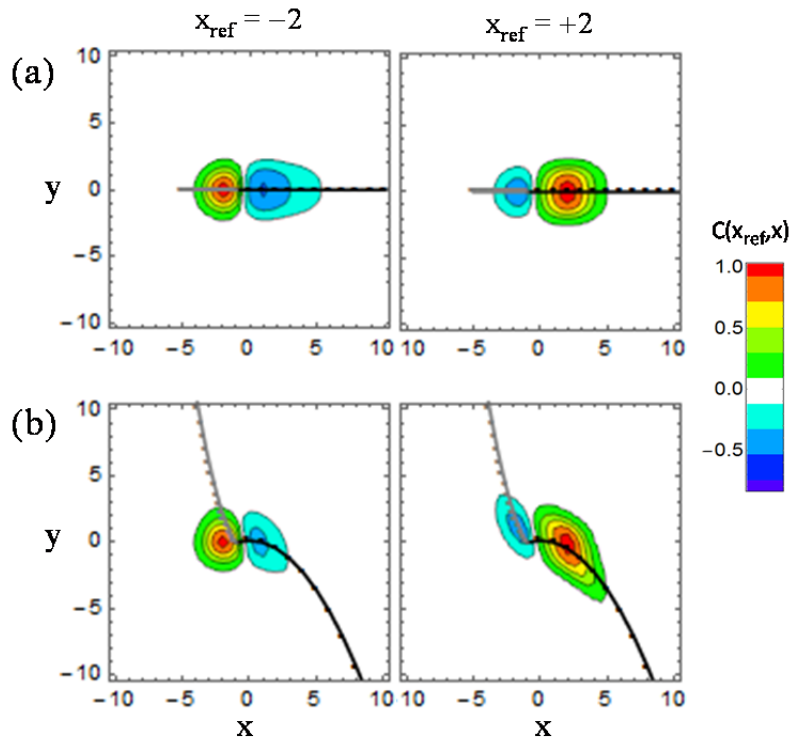| Symbol	Default	Comment
y_0	0.	creation location
δ_y	1.	blob-hole spatial size
v_{by}	0.	blob velocity at $x = 0$
α	0.	velocity shear
v_{hy}	0.	hole velocity

Fig. 6 Effect of sheared flow on the correlations $C(\mathbf{x}_{ref},\mathbf{x})$. In the left panels, the reference point is at x_{ref} = -2, i.e. near the hole; in the right panels x_{ref} = +2, i.e. near the blob. Results are shown for base case parameters (no shear) in (a) and for the sheared flow case with α = 0.3 in (b). In these figures, the trajectories of the blob and hole are superimposed in black and gray lines respectively. Dots indicate positions at time intervals of Δt = 1.

Some additional observations from the 2D correlation studies are not illustrated, and are mostly obvious and similar to the 1D results. Poloidally elongated blobs ($\delta_y > \delta_x$) result in poloidally elongated correlation patterns. Increased noise decreases the magnitude of the negative correlations. A large value of x_{ref} results in negligible negative correlations since the hole by that time has decayed.

5.2 Qualitative reconstruction of NSTX data

The extent to which the model is capable of reproducing qualitative features of the experimental data is indicated in Fig. 7. Part (a) of this figure is the experimental GPI data from NSTX as reported in Ref. [19] for a particular case, discharge #140392, chosen to have good alignment of the GPI optics with the magnetic field. The reference locations for these correlations (center of the red region where the correlation is one) are $x_{ref} = (-6$ cm, -3 cm , 0, $+3$ cm , $+6$ cm) with respect to the separatrix in the five frames. Part (b) of Fig. 7 is obtained from the model using the base case parameters except for $v_{hy} = 1$, $\alpha = -0.3$, $r_{rms} = 0.1$. The corresponding dimensionless reference locations are $x_{ref} = (-4, -2, 0, 2 , 4)$ and y_{ref} is chosen to be on the trajectory (shown at successive times with dots joined by the black/grey line for the blob/hole).

There are a few qualitative similarities between the model and the data: the red/blue "dipole" correlation pattern flips as the reference point moves from the closed surfaces to the SOL; when x_{ref} is large (in the SOL) $|C_{min}|$ becomes small; finally, the patterns are sheared in a similar way. The qualitative agreement is impressive despite the simplicity of the model. It suggests that the basic idea of blob-hole pair creation in a background sheared flow, and subsequent hole decay, may be sufficient to explain many features of the experimental data.

One limitation of the model is seen in the left-most frame of Fig. 7(b), where the blob is outside the viewing area. This is an artifact of using a constant shear. When the reference point is at large negative x, it detects the left-moving hole a long time after the blob-hole pair has been created. At this time the blob has travelled to large positive x and the constant shear model gives the blob ever larger v_y in far SOL, causing it to leave the frame. These large values of v_y in the far SOL resulting from the constant shear model are not realistic for NSTX.
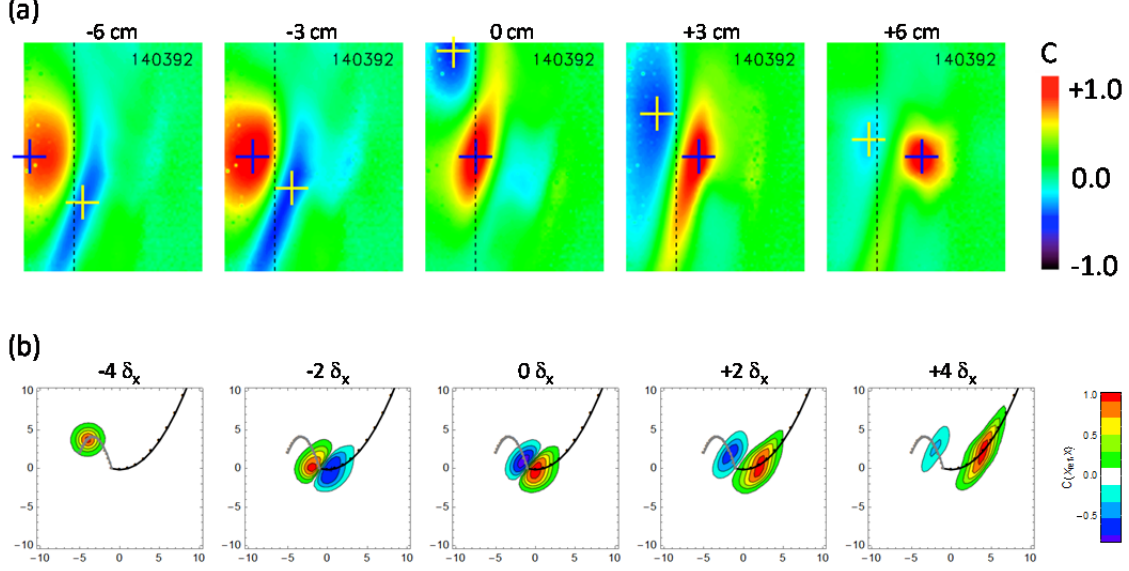
Fig. 7 Comparison of spatial correlation patterns: (a) NSTX GPI data (reproduced with permission from Fig. 7(a) of Ref. [19]). The experimental data spans a range of 24 cm radially (horizontally) x 30 cm poloidally (vertically). (b) a qualitative reconstruction of a similar pattern sequence using the model (dimensionless units). In successive frames moving from left to right the reference point (center of the red region where the correlation is one) moves from the closed surfaces to the SOL.

6. Experimental search for holes

To further investigate the interpretation of the negative correlation features seen in the GPI dataset as resulting from holes, we have applied two other analysis techniques to the experimental data: time delay correlation and minima tracking. These results extend the GPI studies on NSTX reported previously.

Details of the GPI system and the experimental NSTX discharges analyzed in this section were presented in Ref. [19]. In summary the camera took images of the GPI light intensity at a rate of 2.5 μs per frame and 4000 sequential frames were analyzed in each discharge, corresponding to 10 ms. The image plane was resolved by 64×80 pixels covering approximately 24 cm radially (horizontally) and 30 cm poloidally (vertically). Other experimental analysis procedures are the same as described in Ref. [19].

6.1 Time delay correlation

If the negative correlation regions in the data are caused by holes, then the holes should move inwards in time while the blobs move outwards. Time delay correlation

16

provides one method that can be used to search for the relative motion of blobs and holes. The time delay correlation function is defined by generalizing Eq. (1) to

$$C_{12}(\tau) \equiv \frac{\left\langle\left\langle \widetilde{S}(\mathbf{x}_1,t)\widetilde{S}(\mathbf{x}_2,t+\tau) \right\rangle\right\rangle}{S_{1,rms}S_{2,rms}} \tag{16}$$

where, as before, $\widetilde{S}(\mathbf{x},t)$ is the fluctuating part of the signal at position $\mathbf{x}$ and the double angle-brackets represent a long time or statistical average over t.

A sample sequence of time delay correlations from the NSTX GPI dataset is illustrated in Fig. 8 with the reference point held fixed at +3 cm into the SOL at zero time delay. Although one can see some outward motion of the blob (i.e. the positive correlation region), the negative correlation region does not show much radial motion.
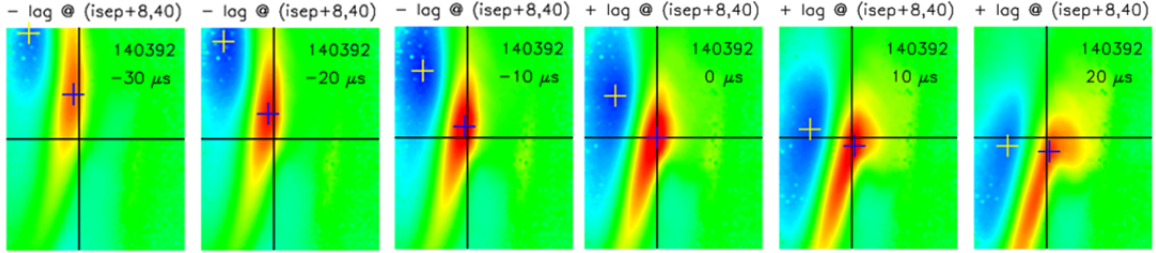

Fig. 8. Sequence of time delay correlations for NSTX discharge #140392. The location of the maximum and minimum correlations in each frame are indicated by the small yellow and blue crosses. The reference point, defined at zero time delay, is at +3 cm and is indicated by the large black horizontal and vertical bars. Thus, the correlation pattern in the 4th panel (0 μs) in this figure is identical to that in the 4th panel (+3 cm) of Fig. 7.

Using the same technique, we have examined other ranges of time delays up to ±50 μs and other correlation reference points (inside and outside the separatrix). Results are quantified in Fig. 9 where the location of the peak positive and negative correlation points are tracked in time for three different reference locations. For these reference locations, we expect from the modeling that the positive correlation should correspond to a blob and the negative correlation to a hole. In all cases the blob moves outward as expected. The negative correlation points show less radial motion, but in apparent contradiction to the model, the observed motion is also dominantly outward. However, the outward motion of the negative correlation point does not appear to follow the motion of the peak positive correlation as it would if it were the result of neutral shadowing.
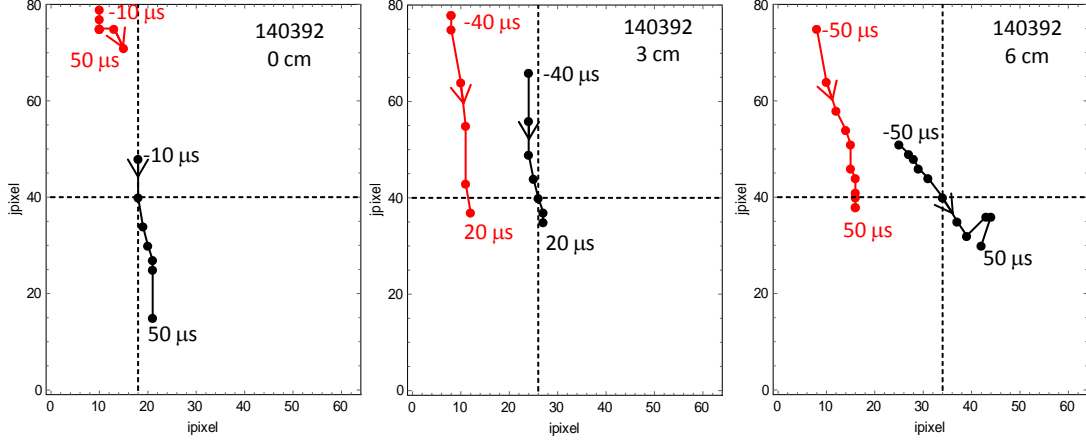
17

Fig. 9. Tracked positions of the maximum and minimum correlations for three different reference locations: 0 cm, 3 cm and 6 cm. Arrows indicate the direction of motion and inset text gives the time lag. Dashed lines indicate the reference location for the correlations. The 3 cm case corresponds to the frames shown in Fig 8.

To verify that the time delay correlation should be capable of detecting relative blob and hole motion, we applied the same analysis technique to synthetic data generated by our blob-hole model. For this test, in addition to assuming random pair creation times and amplitudes, a random distribution of blob sizes, velocities and creation locations in y was assumed. The synthetic data resulting from a statistical sample of 321 blobs in 1001 frames ($\mu = 0.3$) with 64×80 pixel resolution was given as input to the same computer code used to analyze the experimental data. (Note that this procedure is different from the model correlation functions in Secs. 4 and 5 where the statistical averages and correlations were calculated semi-analytically.)

Correlations produced by the synthetic data for a sequence of time delays are shown in Fig. 10 and the positive and negative peaks of these correlations are tracked vs. time and space in Fig. 11. In contrast to Figs. 8 and 9, clear evidence for inward motion of the negative peaks and outward motion of the positive peaks is evident, corresponding to hole and blob motion, respectively.

We conclude that the time delay correlation analysis is indeed capable of detecting relative blob-hole motion, but fails to do so with the NSTX data that we have examined. It is possible that inward motion of holes does not occur; however, this would contradict previous experimental evidence, [10,16] the results of Sec. 6.2 which follow, and theoretical expectations. Thus we are led to consider other explanations.

A comparison of Figs. 8 and 10 shows that the synthetic data is not faithful to the experimental data in at least one critical respect touched on previously in connection with Fig. 7. The correlations in the GPI data are more sheared and/or offset poloidally than in the model. The reason may have to do with the spatial dependence of the flows and the shearing rate. This affects the time development of the blob-hole structures with increasing time lags as the blob and hole become more spatially separated. While the shearing rate can be changed in the model, it must be a constant for the analytical solution given by Eq. (13). This precludes modeling the potentially important effects of the temporal or spatial dependence of the shearing rate.
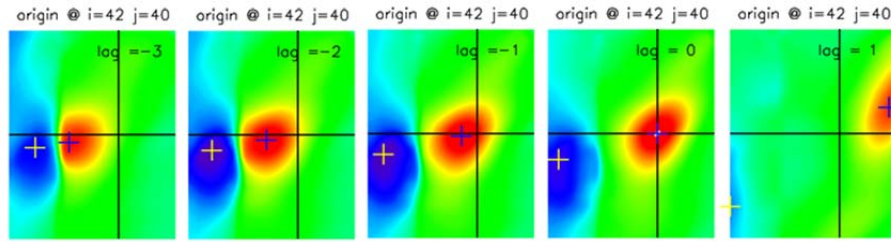

Fig. 10. Sequence of time delay correlations for a synthetic data set produced by the model. See the caption of Fig. 8 for a description of the symbols. Time lags are given as inset text in units of frames.
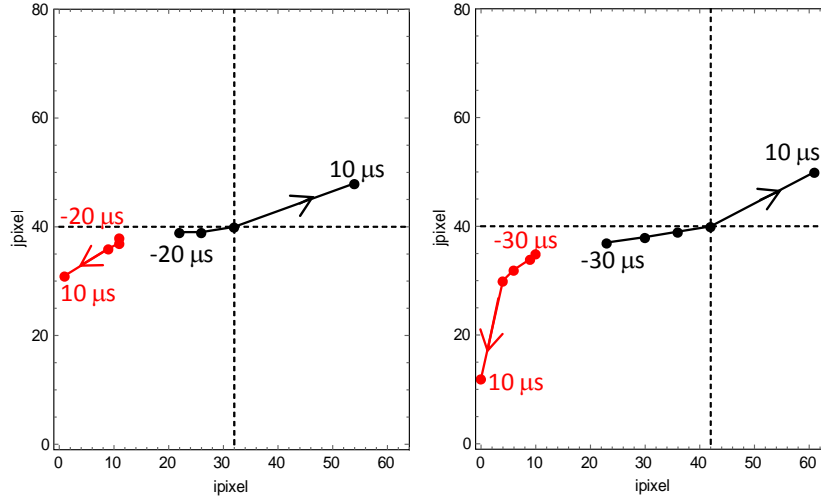

Fig. 11. Tracked positions of the maximum and minimum correlations for two different reference locations using the synthetic data. Dashed lines indicate the reference location for the correlations, inset text gives the time lag and arrows indicate the direction of motion. The right panel corresponds to the frames shown in Fig 10.

19

6.2 Minima tracking

We show, in this section, that local minima, i.e. negative peaks in the normalized GPI intensity, can be tracked and that on average they move inward while the maxima move outwards, both as expected from theoretical considerations. Although holes are expected to be local minima, there is no implication of negative skewness for these minima. The minima tracking algorithm employed in this section does not attempt to identify blob-hole pairs; however, these negative peaks do not appear to be shadows of the blob that move outward with it. We note that holes (also called voids or negative intermittent plasma objects) have been observed in previous experiments using probes [10,16].

As with the correlation analysis, the tracking analysis begins by normalizing all data to a time-averaged frame over 10 ms of interest, and then spatially smoothing over 3 pixels (~ 1 cm). The minimum and maximum values of the normalized GPI intensity for each frame are then determined within a region of interest defined by ±6 cm (±16 pixels) with respect to the local separatrix radially and ±11 cm (±30 pixels) with respect to the image center poloidally. The velocity is determined by the jumps in the extrema between frames, where only jumps of less than 6 pixels/frame (9 km/s) are retained in the database. Also excluded from the database were extrema for which the minimum in a frame was radially outside the maximum in that frame, and extrema within 1 pixel from the edges of the region of interest.

For a fixed pixel located in the SOL, the signal exhibits positive intermittent events in time as expected corresponding to the propagation of blobs past the observation point. However, when the observation point is inside the separatrix, the GPI signal is rather symmetrical in positive and negative pulses, showing little evidence for negative skewness. This is in contrast to probe observations [16] and is one reason why detection of holes appears to be more difficult with GPI. Sample signals are shown in Fig. 12.
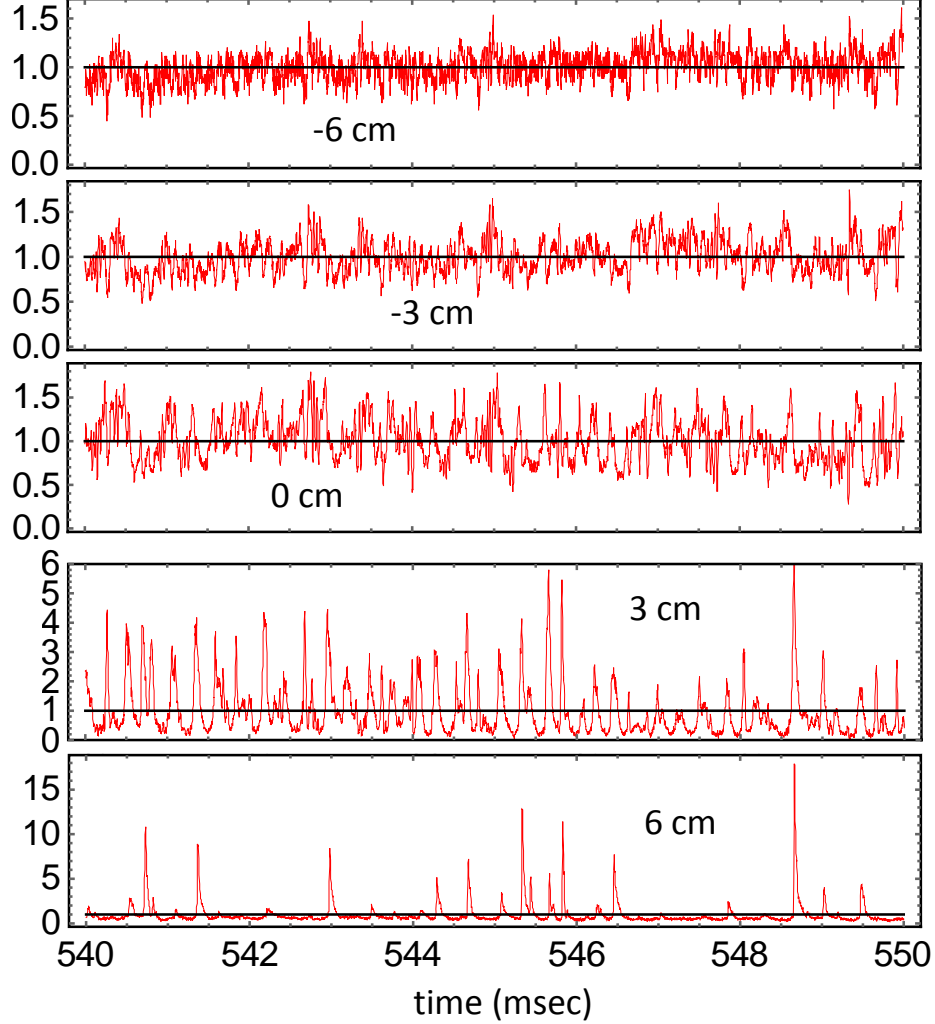
Fig. 12.Time histories of normalized signal levels for discharge #140392 at five different locations with respect to the EFIT separatrix, as indicated by the inset text. The horizontal solid black line is the mean over time. Positive skewness is evident outside the separatrix.

Figure 13 shows histograms of the normalized signal amplitude and the velocities of maxima and minima obtained by tracking their motion between successive frames. The signal amplitude in Fig. 13 (a) has a broad distribution about its maximum extending close to zero and nearly symmetric about the maximum close to the location of the peak. This is consistent with the lack of negative skewness in the time histories of Fig. 12. On the other hand, while the signal cannot go negative, it can extend to large positive values in the tail, which is consistent with the positive skewness seen in Fig.12.

Results for the radial velocity distributions of the maxima and minima for shot #140392 are given in Figs. 14(b) and (c), in units of pixels/frame. The median values of

the amplitudes of the 869 extrema for this shot were 0.36 for the minima (in normalized signal units) and 3.2 for the maxima. The radial velocities of the maxima and minima both have relatively broad distributions, but the mean velocity of the maxima is +575 m/s (outward) and the mean velocity of the minima is −308 m/s (inward). This suggests that the minima tend to move inward like holes while the maxima tend to move outward like blobs, as expected qualitatively from the blob-hole model.
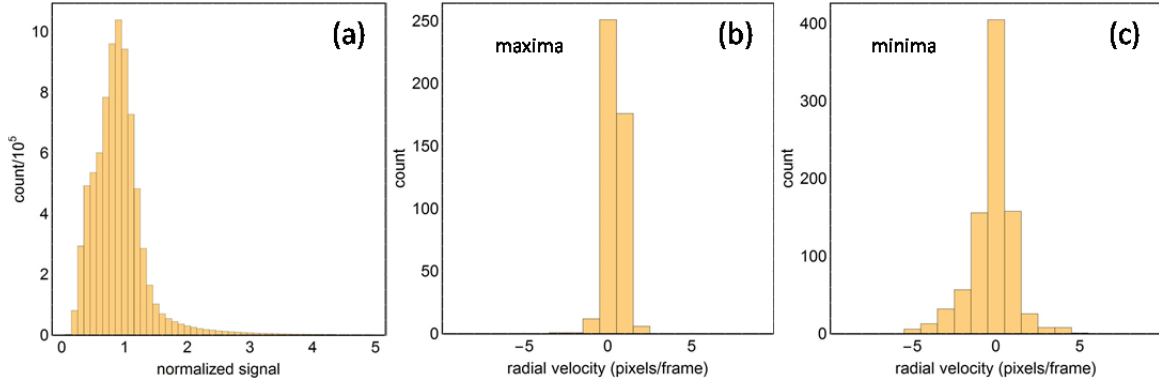

Fig. 13 Histograms of (a) the normalized signal amplitude, and the change in radial pixel location per frame for (b) maxima and (c) minima. In (b) and (c) a change of one radial pixel per frame corresponds to a radial velocity of 1.5 km/s. Data is for discharge #140392.
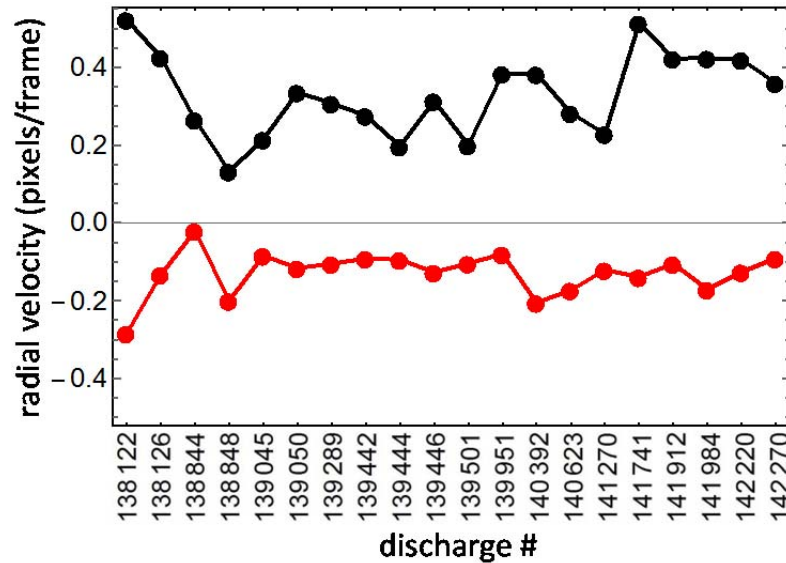

Fig. 14 Summary of average velocities of the minima and maxima for 20 discharges in the database, including shot 140392 used in Fig. 13. The mean maxima (minima) velocity is positive (negative) in all cases. One pixel per frame corresponds to a radial velocity of 1.5 km/s.

Finally, Fig. 14 presents a summary of the mean velocities if the minima and maxima for all 20 shots in the database employed in Ref. [19]. Discharge #140392, singled out for study in many of the previous figures, has fairly typical extrema velocities. The evidence for net inward motion of the minima is quite compelling.

Although the mean outward motion of the normalized signal maxima and the mean inward motion of the normalized signal minima are qualitatively consistent with the theoretical expectation for the radial motion of blobs and holes respectively, it should be emphasized that this analysis did *not* specifically identify the theoretically expected blob-hole pairs in the GPI data. Even though the database contained only extrema with their maxima at a larger radius than the minima, the most of these minima (e.g. in shot 140392) were located outside the separatrix, where the relative fluctuation level was the largest. In contrast, if holes are created as voids left in the plasma as the blobs are created and propagate away, then one might expect hole detections to occur primarily inside the separatrix or near the blob birth location. Also, the average (total) separation between minima and maxima in a given frame was ~12 cm or 32 pixels (for shot #140392), which is significantly larger than the blob correlation length of ~3-5 cm [9]. In contrast, the blob-hole modeling in Figs. 6 and 7 suggests that the holes should be most evident when they are near the blobs. Furthermore, the individual separations between minima and maxima show no obvious correlation with either their radial position or their velocity, and the radial velocities of the extrema showed no significant variation with respect to their magnitude, as might be expected from the blob-hole model.

We close this section with an additional comment about the skewness in the GPI data. All of the 20 discharges of Fig. 14 have high positive skewness outside the separatrix, and 18 of these discharges also have small positive skewness (~ 0 to 1) inside the separatrix (with two shots having small negative skewness there). This is consistent with the near-absence of negative skewness previously seen in GPI data [55]. Because of the nonlinearity of the GPI intensity as a function of density and temperature, the skewness measured by GPI may not be simply related to the skewness of density or ion saturation current fluctuations as measured by probes. Thus the presence or absence of skewness in the present dataset is inconclusive with respect to the presence of density holes.

7. Discussion and conclusions

In this paper we have presented a simple model for the creation of blob-hole pairs which are presumed to evolve through a continuity equation in the presence of background flows. This blob-hole pair model was then employed in a statistical theory to calculate the spatial correlation function. Poisson statistics was assumed for the blob-hole waiting time distribution, and, less critically, the initial amplitude of the blob-hole pair was assumed to be exponentially distributed. The latter assumption only affects the normalization of a Gaussian white noise background, meant to simulate background edge turbulence that is unrelated to the blob-hole pairs.

It was found that in this model the correlation patterns were sensitive to the blob-hole spatial extent, the random background noise level relative to blob/hole production rate and lifetime, sheared flows and the hole velocity and lifetime relative to that of the blobs.

The blob-hole model qualitatively reproduced several features of the experimental GPI 2D spatial correlations: dipole correlation patterns in the direction of blob-hole propagation that "flip" depending on the location of the reference point; negative correlations of varying magnitude depending on background "noise" and the location of the reference point; and sheared correlation patterns. In general the model produced correlation patterns that were qualitatively consistent with an interpretation of the GPI data as resulting from blob-hole pairs.

Motived by this finding, we reexamined the experimental gas puff imaging dataset to look for more direct evidence for the existence of holes and their postulated inward motion. Two methods were considered.

A time delay cross-correlation analysis was applied to both the synthetic data from the model and the experimental GPI data. For the synthetic data, this analysis revealed the inward motion of holes and the outward motion of blobs that was built into the model. In contrast, for the GPI data the peak negative correlation regions were not found to move in the opposite direction from peak positive correlation regions as would be expected for blob-hole pairs. Neither did they closely follow the motion of the peak positive correlations as would be expected if neutral shadowing were the explanation. It was suggested that strong temporal or spatial variations of the velocity shear, not present in the synthetic data, may play a role in the different behavior of the experimental and synthetic data using this analysis method.

A second experimental analysis of holes used a tracking technique based on the motion of minima and maxima of the normalized GPI signal. This analysis revealed clear evidence for the mean outward motion of maxima and the mean inward motion of minima. The latter is a new result for a GPI analysis in NSTX. However, the present analysis technique, being based on the global extrema of each frame, did not directly attempt to attribute the maxima and minima to blob-hole pairs. In fact, several of the data analysis results were qualitatively inconsistent with the blob-hole modeling: the relative separation of the minima and maxima were rather large in most frames; the minima were not dominantly inside the separatrix; almost half of the minima were observed to have an outward directed radial velocity; and there was no clear variation of the radial velocity with the magnitude of the extrema. Furthermore, most of the discharges examined did not exhibit any negative skewness of the GPI signal, as seen in probe data for holes.

The search for direct experimental evidence for holes in the GPI data by these two methods is thus somewhat inconclusive and inconsistent. A partial explanation may be that the correlation method averages over all structures, while the extrema method tracks only the very tip of the negative distribution in the normalized signals, which can be more sensitive to slight inward motion.

In conclusion, we have seen that 2D correlation patterns are useful to give a broad range of properties in a single image: radial and poloidal correlation lengths, the presence or absence of sheared flows, and according to the modeling, the presence or absence of blob-hole pairs. Other methods, such as time-delay estimation, tracking and conditional sampling, may be good alternatives to analyze specific properties in detail. In particular further studies of minima and their possible identification as holes, their propagation characteristics, relationship to plasma regimes and discharge conditions, and to velocity shear would be of interest for future work. In addition to improving our understanding of edge turbulence in general, hole propagation may be of interest to understand possible turbulence spreading from the separatrix region into the pedestal.

Acknowledgments

References

1 Lipschultz B *et al* 2007 Nucl. Fusion **47** 1189
2 Connor J W *et al* 1999 Nucl. Fusion **39** 169
3 Chang C S *et al* 2017 Nucl. Fusion **57** 116023
4 Halpern F D *et al* 2017 Phys. Plasmas **24** 072502
5 Myra J R *et al* 2016 Phys. Plasmas **23** 112502
6 Krasheninnikov S I 2001 Phys. Lett. A **283** 368
7 Krasheninnikov S I *et al* 2008 J. Plasma Phys. **74** 679
8 D'Ippolito D A *et al* 2011 Phys. Plasmas **18** 060501
9 Zweben S J *et al* 2016 Plasma Phys. Control. Fusion **58** 044007
10 Boedo J A *et al* 2003 Phys. Plasmas **10** 1670
11 Carralero D *et al* 2014 Nucl. Fusion **54** 123005
12 Vianello N *et al* 2017 Nucl. Fusion **57** 116014
13 Militello F *et al* 2013 Plasma Phys. Control. Fusion **55** 025005
14 Zweben S J 1985 Phys. Fluids **28** 974
15 LaBombard B *et al* 2014 Phys. Plasmas **21** 056108
16 Boedo J A *et al* 2014 Phys. Plasmas **21** 042309
17 Zweben S J *et al* 2017 Rev. Sci. Instruments **88** 041101
18 Zweben S J *et al* 2015 Nucl. Fusion **56** 093035
19 Zweben S J *et al* 2017 Phys. Plasmas **24** 102509
20 Stotler D B *et al* 2003 J. Nucl. Mater. **313-316** 1066
21 Wersal C *et al* 2017 Nucl. Fusion **57** 116018
22 Garcia O E 2012 Phys. Rev. Lett. **108** 265001
23 Angus J R *et al* 2012 Phys. Plasmas 19 082312
24 Walkden N R *et al* 2016 Plasma Phys. Control. Fusion **58** 115010
25 Easy L *et al* 2014 Phys. Plasma 21 122515
26 Stepanenko A A *et al* 2017Phys. Plasmas **24** 01230
27 Bisai N *et al* 2012 Phys. Plasmas 19 052509
28 Manz P *et al* 2013 Phys. Plasmas 20 022308
29 Russell D A *et al* 2015 Phys. Plasmas 22 092311
30 Madsen J *et al* 2011 Phys. Plasmas 18 112504
31 Wiesenberger M *et al* 2014 Phys. Plasmas 21 092301
32 Hasegawa H and Ishiguro S 2017 Nucl. Fusion **57** 116008
33 Bodi K *et al* 2008 Phys. Plasmas 15 102304
34 Kendl A 2015 Plasma Phys. Control. Fusion 57 045012
35 Riva F *et al* 2016 Plasma Phys. Control. Fusion **58** 044005
36 Zhang Y and Krasheninnikov S I, 2016 Phys. Plasmas **23** 124501
37 Ricci P *et al* 2012 Plasma Phys. Control. Fusion **54** 124047
38 Zhu B *et al* 2017 Phys. Plasmas **24** 055903
39 Umansky M V *et al* 2009 Comput. Phys. Commun. **180** 887
40 Dudson B D and Leddy J 2017 Plasma Phys. Control. Fusion **59** 054010
41 Galassi D *et al* 2017 Nucl. Fusion **57** 036029
42 Bisai N and Kaw P K 2016 Phys. Plasmas **23** 092509

43 Russell D A *et al* 2016 Phys. Plasmas **23** 062305

44 Ku S *et al* J. 2016 Comput. Phys. **315** 467

45 Garcia O E *et al* 2015 Nucl. Fusion **55** 062002

46 Theodorsen A *et al* 2017 Nucl. Fusion **57** 114004

47 Militello F and Omotani J T 2016 Nucl. Fusion **56** 104004

48 Walkden N R *et al* 2017 Plasma Phys. Control. Fusion **59** 085009

49 Garcia O E *et al* 2016 Phys. Plasmas **23** 052308

50 Xu G S *et al* 2009 Nucl. Fusion **49** 092002

51 Cheng J *et al* 2010 Plasma Phys. Control. Fusion **52** 055003

52 Nold B *et al* 2010 Plasma Phys. Control. Fusion **52** 065005

53 Yan N *et al* 2013 Plasma Phys. Control. Fusion **55** 115007

54 Simon P *et al* 2014 Plasma Phys. Control. Fusion **56** 095015

55 Sattin F *et al* 2009 Plasma Phys. Control. Fusion **51** 055013

56 Carter T A 2006 Phys. Plasmas **13** 010701

57 Fisher D M *et al* 2015 Phys. Plasmas **22** 092121

58 Iraji D *et al* 2010 Phys. Plasmas **17** 122304